Low Pressure Sand Casting of Ultrasonically Degassed Al7SiMg Alloy: Modeling and Experimental Validation of Mould Filling

H. Puga[1*], J. Barbosa[1], T. Azevedo[2], S. Ribeiro[2], J. L. Alves[1]

[1] Centre for Micro-Electro Mechanical Systems, Department of Mechanical Engineering, University of Minho, Campus of Azurém, 4800-058 Guimarães, Portugal

[2]FEUP, Department of Metallurgical and Materials Engineering, 4200-465 Porto, Portugal

*Corresponding author: H. Puga (PhD) – puga@dem.uminho.pt

Tel: +351253510220; Fax: +351253516007

Abstract

The effect of combining smooth mould cavity filling and ultrasonic degassing by using a low pressure sand casting process with US melt treatment on the microstructure and mechanical properties of A356 alloy was investigated. Computational fluid dynamics (CFD) modelling and experimental validation was used to study the liquid metal flow behaviour and oxide film defect distribution for different filling rates, using two pressurization curves (p-t). The effect of ultrasonic degassing on the resultant microstructure (morphology and presence of porosities and inclusions) was studied for 650 and 700ºC melt degassing temperatures. Results show that ultrasonic degassing and mould filling velocities below 0.5 m/s improve the alloy microstructure and lead to high mechanical properties.

Keywords

Simulation, Ultrasonic degassing, Low Pressure Sand Casting, Mechanical properties, Oxides

1. Introduction

Low Pressure Die Casting (LPDC) is a consolidated process that has been widely applied in the foundry industry for producing light alloy castings which request high mechanical performance. The process presents some advantages, such as smooth mold filling and feeding capacity [1]. Although die casting is very competitive for manufacturing aluminium alloy components [2], the

cost of manufacturing and modification of mold design and the impossibility of heat treating the castings due to blister formation at the surface are considered the major drawbacks of this process. Moreover, although certain geometries can be produced by die casting, medium and large parts are usually obtained by sand casting. Sand casting is a simple way to manufacture Al castings with complex geometries, able to suffer heat treatment, but they are very susceptible to the presence of inclusions [3] and coarse microstructures [4] due to low cooling rates and turbulent filling, respectively. The majority of metalcasting facilities operating in open atmosphere easily oxidizes the melt surface and creates an oxide film which trend to be ruptured during pouring. Furthermore if the liquid velocity during casting is high enough (typically more than 0.5 m/s), the flow surface becomes turbulent, thus presenting tendency to fold and entangles new oxide films that will be present after solidification causing degradation of the casting properties (see e.g. [5] and [6]). Moreover, according to Cáceres *et al*. [7] the entrapped oxide films are frequently accompanied by different casting defects such as shrinkage pores and dross.

One way to avoid inclusions can be to adapt the low pressure die casting process to sand casting. Using pressure differential, the melt can rise smoothly into the mould cavity through a pipe, avoiding dross pickup and turbulence, ensuring high and consistent casting quality since oxide films and inclusions are largely eliminated. Therefore, the castings possess high density, high soundness and good mechanical performance.

Regarding to porosity and coarse microstructures, these can be controlled by ultrasonic degassing/refinement, which is an extremely efficient and environmentally friendly technique, based on the supply of acoustic energy to the molten metal in order to induce cavitation at different stages of the casting process (see e.g. [8],[9],[10] and [11]).

This work has introduced new developments in the Low Pressure Sand Casting process which combines low pressure pouring, sand casting and ultrasonic degassing concepts. The proposed process is extremely important to increase the performance of Al casting since it will increase the soundness and mechanical properties of final castings.

The main objective of this study is to investigate the effect of mould filling parameters on the mechanical strength of Al7SiMg alloy castings, focusing on the relationships among the liquid aluminium flow behaviour, presence and distribution of oxide films, microstructure and ultimate strength. Computational fluid dynamics (CFD) modelling is used to investigate the

liquid metal flow behaviour for different filling rates, which were experimentally validated. It is also characterized the effect of ultrasonic degassing on the as-cast microstructure. Scanning electron microscopy (SEM) is used to characterize the alloy microstructure features and to identify macro and microstructure defects. The Weibull statistics method is employed to quantify the effects of different pressurizing rate and US degassing temperature on the ultimate strength and reliability of castings.

2. Computational Modeling

Numerical simulation has been performed to study the filling cavity behavior, in order to predict the velocity of the melt for the different pressure-time (*p*-*t*) curves. The filling model involved the development and testing of a computer model based in new concept to simulate the low pressure process - Element Compressor - developed within the framework of the NovaFlow&Solid package.

2.1 Governing equations – Fluid Flow Simulation

Generally, the molten flow in processes under low pressure conditions is considered as a laminar flow, incompressible, which means that the density of the fluid does not change in time or space under pressure or temperature. Moreover, in the present case the motion of fluid is governed by the principles of classical mechanics and thermodynamics for the conservation of mass, momentum and energy. Thus, the basic equations for the mass conservation law may be written as:

$$\frac{\partial \rho}{\partial t} + \partial_i \left(\rho v_i \right) = 0 \qquad (1)$$

where ρ is the mean density and v_i is the component of mean flow velocity. The momentum conservation law may be written as:

$$\frac{\partial \rho}{\partial t} + \partial_j \left(\rho v_i v_j \right) - \partial_j \left(\mu \left[\partial_i v_j + \partial_j v_i \right] \right) = -\partial_i p - \rho g_i \qquad (2)$$

where g_i is the components of free fall acceleration. It is assumed for the mean density that equations of stat form

$$\rho = \rho(p,T) \qquad (3)$$

are known and dependent of $\mu = \mu(T)$

Boundary conditions are required to solve the mass and momentum equations. The importance of these boundary conditions is critical to stability and convergence of results. Thus, equations (1) and (2) should be solved considering the following conditions: (i) sticking on the solid boundary ($\vec{v} = 0$); (ii) slipping on the symmetry plane ($v_n = 0$) and (iii) absence of forces ($\sigma_{ik} n_k = 0$).

Additionally, to describe the mould filling cavity at low pressure in NovaFlow&Solid, the approximate dynamic system is used.

$$\frac{d}{dt} J = \frac{1}{\sum_{i=0}^{1} \frac{h_i(t)}{S_i}} \sum_{i=0}^{1} \left[(-1)^i \left(p_i(t) + \rho g h_i(t) + \frac{(\beta_i + 1) J^2}{2\rho S_i^2} \right) - \frac{J K_i h_i(t)}{S_i} \right] \qquad (4)$$

Equation 4 is the result of the integration of moment conservation law, considering the laminar flow and entering the liquid flow J via the transverse tube section. p_i is referred to pressure on the surface, S_i refer to the area of transversal section, K_i the Stock's resistance and β_i is the effective resistance owing to flow turning. Considering that some turbulence can occur during filling, NovaFlow package take in account the standard K-e module which considers the possibility of a turbulent flow, taking into account a more adequate description of flow characteristics, affecting k values of equation 4. The basic equation for standard K-e module have the form:

EQUATION (5)

2.2 Modelling setup

The model was developed according to the new concept to simulate the low pressure casting – Element Compressor. To use this new approach it is necessary to include the following elements in the numerical model: (1) casting; (2) camera around sand mold; (3) sand mold; (4) sprue; (5) crucible; (6) melt in the crucible and (7) camera around

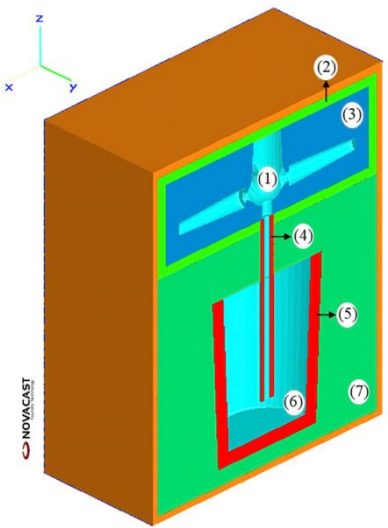

the crucible, according to Fig. 1.

Fig. 1. Model of casting layout.

Fig.2 shows the geometry of the mould cavity, which was imported into NovaFlow&Solid. The control volume mesh (CVM) consisting of 6557760 cells with 1.4mm of dimension of cell was automatically generated. A standard Al-Si alloy (Al7Si0.3Mg) whose thermo-fluid dynamics properties needed for simulation are well known was considered [12]. One virtual sensor (S#1) for fluid velocity characterization was inserted in the numerical model. S#2 refers to the position where cast samples microstructure was evaluated.

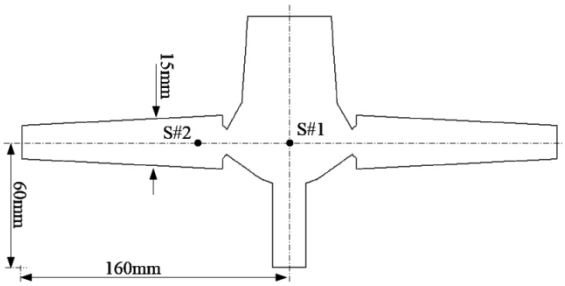

Fig. 2. Geometric model where S#1 and S#2 are the sensors.

2.3 Initial and boundary conditions

Contrary to what is expected in the Low Pressure Die Casting process, where the initial temperature in the die is not uniform in the first cycles [13], in this new approach the initial temperature of sand mould is uniform - room temperature - and the same in every cycles since a new mould is always used.

The temperature of the incoming fluid is influenced by the rate at which heat is lost to the surroundings of the rise tube. Since the rise tube is fairly insulated, it is safe to assume that the incoming fluid temperature is similar to the temperature of the metal inside the crucible.

In 3D sand casting model each of the 6 mould boundaries must be defined. Thus the lateral boundaries (plane YZ and ZX, according to Fig. 1) were considered with heat transfer defined by the coefficient between mould and external environmental. A constant temperature of 80 ºC was considered for the lower plane XY (boundary between sand mould and sealing cap). In what concerns to the upper plane YZ it was considered that heat is lost by radiation and convection (open feeder).

The fluid flow at the ingate can be defined by either a velocity or pressure boundary condition. The velocity can be estimated from the experimental filling time according following equation:

$$v_i = \frac{V_c}{t_f S_i}, \qquad (5)$$

where v_i is the velocity at the ingate, V_c is the volume of the casting, S_i is the cross-sectional area of the ingate and t_f is the filling time. However the use of velocity only can be made when the filling time is known in advance. How in present case the velocity and filling time are the variables to estimate, then the pressure boundary condition must be used. Table 1 presents the parameters of the pressure-time (p-t) curves used for mould filling.

Table 1. Parameters of the pressure-time (p-t) curves used for mould filling.

Pressure curve	M1 (0 – 5 s)	M2 (5 – 10 s)	M3 (10 – 15 s)	M4 (15– … s)	Observation
(1)	1400 Pa/s	400 Pa/s	0	0	Curve with 2 ramps
(2)	600 Pa/s	400 Pa/s	800 Pa/s	0	Curve with 3 ramps

3. Experimental Procedure

3.1 Experimental set-up and procedure

An electrical melting furnace equipped with a SiC crucible of 15 kg capacity, adapted to the low-pressure sand casting (LPSD) was used. The top of the furnace is covered with a removable

steel plate that seal the melting chamber and supports the sand mould which has a top atmospheric riser. The plate has a central hole to allow the introduction of a tubular ceramic acoustic radiator to perform melt degassing and the ceramic pipe that allows the liquid metal to rise into the mould, according to Fig. 3.

The Al7Si0.3Mg alloy was melted and held inside the crucible at different pouring temperatures during 30 minutes for homogenization. US degassing vibration based in MMM technology [11] was applied, after which the US unit was stopped. MMM technology (multi-frequency, multimode, modulated technology) is characterized by synchronously exciting many vibration modes through the coupled harmonics and sub-harmonics in solids and liquid containers. This technology produces high intensity multimode vibration that are uniform and repeatable, which avoid the creation of stationary and standing waves, so that the whole vibrating system is fully agitated, improving cavitation.

The pressure inside the furnace was then increased over the atmospheric pressure to make the melt rise into the mould cavity, according to different experimental conditions presented in Table 2.

Pressure and pressurizing curves were controlled by a specially designed set of electromagnetic and pneumatic valves using LabView software. Melt temperature was controlled within an accuracy of ±5 ºC.

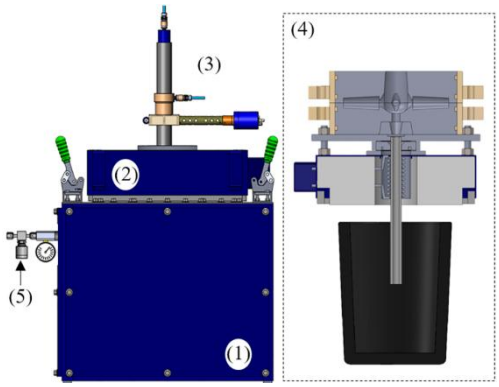

Fig. 3. Experimental set-up of LPSC process. (1) Electrical furnace; (2) Sealing cap; (3) US-degassing system; (4) Device for filling mould; (5) Pressurizing gas.

Table 2. Experimental conditions.

Test Nº.	Temperature (ºC)	Ultrasonic parameters			Pressure curve (see Table 1)
		Time (min)	Frequency (kHz)	Amplitude (μm)	
1	650	0-1-3-5-9	20.1±0.1	40	(2)
2					(1)
3	700	0-1-3-5			(2)
4					(1)

For every experiment, the Reduced Pressure Test (RPT) and the apparent density measurement method were used to evaluate the samples density.

3.2 Samples characterization

Samples for microstructures characterization were taken from every cast samples by sectioning them perpendicularly to its longitudinal axis at the position of sensor #2 (Fig. 2). They were ground using 1200 μm SiC and polished up to 1 μm. Optical microscope (OM) and Scanning Electron Microscope (SEM) were used for characterization.

For tensile testing, after T6 treatment [14] (one of the more commercially common heat treatments for Al7Si0.3Mg), the specimens were machined according to EN 10002-1:2004 with gauge length L_0 of 50 mm and cross section diameter d_0 of 10 mm. Tensile tests were carried out at room temperature on an Instron-Model 8874 testing machining using 0.5mm/min strain rate.

Weibull distribution was used to model extreme values of fracture strength. It is proved that the Weibull distribution can be used to predict the probability of fracture [15]. Although current forms of this distribution can use two or three parameters, in this work was used two-parameter, which is accepted for fracture strength studies [16] . The cumulative probability function of the Weibull distribution is determined by the following equation [1]:

$$p_f = 1 - \exp\left[\left(\frac{\sigma - \sigma_T}{\sigma_0}\right)^m\right] \quad (6)$$

Where σ is the stress, σ_T is the threshold value below which no specimen is expected to fail, σ_0 is the scalar parameter, and distribution shape parameter, m, is the Weibull modulus. If the

threshold value σ_T is zero and re-arranging the equation 6, the two-parameter Weibull distribution can be plotted as a straight line, as follows:

$$\ln\left[\ln\left(1/\left(1-P_f\right)\right)\right] = m\ln\left(\sigma\right) - m\ln\left(\sigma_0\right) \qquad (7)$$

The density of the melt, the metallographic microstructure and mechanical properties taken from cast samples were correlated in order to verify the accuracy of the simulation results with the experimental results and to predict the most suitable cavity filling pressure-time curve to ensure high castings sanity.

4. Results and Discussion

4.1 Numerical results

Numerical simulations were conducted for conditions similar to those of the experiments. The casting parameters, material properties and boundary conditions were computed based on equations presented in the previous sections.

Two pressure-time curves were evaluated according to the parameters presented in Table 1. In contrary of the traditional process (LPDC) where after filling the cavity there is a ramping of increase pressure to applied and held to assist in feeding of the casting [17] and [18], in pressure curves studied this ramps was not considered since the sand mould presents a top atmospheric feeder for interdendritic feeding. Moreover, as the mould cavity is open due to presence of the atmospheric feeder, the final pressure after mould filling was adjusted only to compensate the metallostatic head pressure of the column of fluid: p(t)=ρgh.

Fig. 4 and 5 present the average melt velocity inside the mould cavity registered in sensor S#1 (Fig. 2) for 2 different pressure-time curves at temperature of 700 and 650 ºC, respectively.

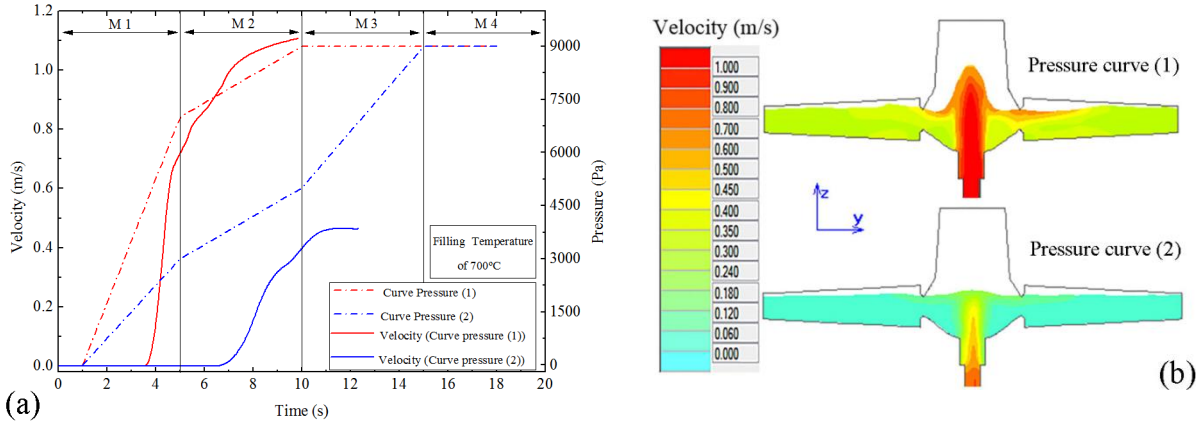

Fig. 4. Numerical results of mould filling simulation for 700 ºC casting temperature. (a) Average melt velocity of filling registered in sensor S#1 during cavity filling; (b) flow chart of velocity in cavity for a filling of 70%.

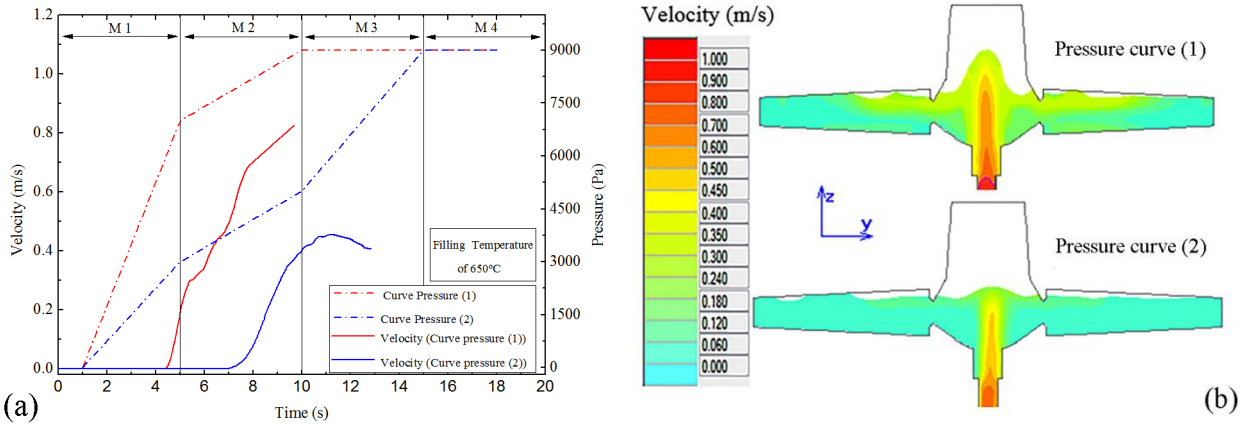

Fig. 5. Numerical results of mould filling simulation for 650 ºC casting temperatures. (a) Average melt velocity of filling registered in sensor S#1 during cavity filling; (b) flow chart of velocity in cavity for a filling of 70%.

The mould cavity is filled by applying pressure to the surface of the liquid metal in the crucible placed inside a melting chamber, according to Fig. 3. It is notorious that the pressure curve (1) has just two ramps while in pressure curve (2) an intermediate ramp was introduced. The intermediate ramp in pressure curve (2) proved to be very important to slow down the filling of the lateral specimens for velocities lower than 0.5 m/s for both melt temperatures.

Although the velocity of the fluid cannot be used to simulate defects, it can be used to estimate the chance to occurrence of surface turbulence. It is recognized by the scientific community that turbulent filling favors the folding of the metal front leading to the formation of additional young oxides as well as their re-incorporation into the bulk of liquid. On this study the use of numerical simulation to establish the pressure-time curve to fill the mould cavity revealed to be extremely important to obtain filling velocities suitable for sand moulds and to reduce oxide formation, without impairing the cavity filling itself. Numerical results also allowed to predict

that total filling of the mould cavity was completed before reaching 5% of complete solidification. Thus, with these interactive simulation it was possible to predict the filling behavior for different pressurizing rate and to select the most convenient filling parameters to obtain sound castings.

4.2 Experimental results

The simulated parameters were tested in the LPSC process experimental set-up presented in Fig. 3. To assess the effect of the different pressure-time curves in the filling of mold cavity the Al7Si0.3Mg melts were degassed before pouring at the desired temperature (Table 2) using the MMM ultrasonic technology [19], to ensure that the density level of bath was identical for every experiment.

The degassing rate by ultrasound is sensitive to melt temperature and increase directly with it, as demonstrated by Fig. 6. Although the results show that for melt temperatures of 650 and 700 ºC the density steady-state plateaus are quite similar (2.65 and 2.66 kg/m^3, respectively), the degassing rate at 650 ºC is lower when compared with that obtained at 700 ºC. For low melt temperature, the high viscosity will stickle the pulsation of the cavitation bubbles, their coagulation and floating [8] and [11]. Thus the diffusion coefficient of hydrogen in the liquid metal decreases with decreasing temperature as well as the diffusion rate of hydrogen from liquid to bubbles. Hence, in order to increase the final density of melts US degassed at low temperatures it is necessary to use higher degassing times.

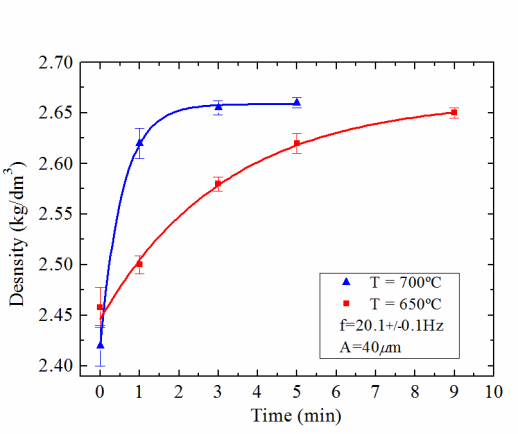

Fig. 6. Average density of the Al7Si0.3Mg as a function of melt temperature and processing time, for 20.1±0.1 kHz and 40 μm of the amplitude of system, evaluated for all experiments.

Fig. 7 presents the microstructure of samples taken from sensor #2 position (Fig. 2) for both casting temperatures and for different pressure-time curves, as presented in Table 1. According to this figure it is quite clear that using pressure curve (2)(Figs. 7 (a) and (c)) promotes the sanity of samples in what concerns to porosity, for both casting temperatures. On the other hand, the use of pressure curve (1) is favorable to arising of interdendritic porosity Fig. 7 (b) an (d). Taking into account that the average alloy density was similar for both pouring temperatures (Fig. 6), it is suggested that porosity is a consequence of turbulent filling caused by high filling velocities. For the sake of comparison, Fig 7 (e) and (f) show the microstructure of cast samples poured at 650 and 700ºC without any degassing treatment, where a coarse dendritic structrure and large gas porosities can be seen. Moreover, the microstructure of those samples seem not to have been affected by the pouring temperature, since no significant diferences in grain size and morphology are detected.

This double effect - degassing and refinement - of US in liquid aluminium can be explained as follows:

(1) Degassing - When a liquid metal is submitted to high intensity ultrasonic vibrations, the alternating pressure above the cavitation threshold creates numerous cavities in the liquid metal. Cavitation intensifies mass transfer processes accelerating the diffusion of hydrogen from the melt to the developed bubbles. As acoustic cavitation progresses with time, adjacent bubbles touch and coalesce, growing to a size sufficient to allow them to rise up through the liquid, against gravity, until reach surface, thus promoting melt degassing.

(2) Refinement - The effect of high acoustic intensity on the grain refinement can be attributed to cavitation-enhanced heterogeneous nucleation. During US degassing, the alternating pressure achieved by MMM ultrasonic processing of liquid metal creates cavitation bubbles able to absorb kinetic (thermal motion) energy in the melt, remaining thermodynamically stable in the molten alloy. Thus, during cooling those thermodynamically stable bubbles remain in the melt and lead to the development f numerous solidification nuclei that induce heterogeneous nucleation and the formation of a large number of globular grains with small grain size. As every experiment was performed with the melt above the *liquidus* temperature, grain refinement and absence of dendritic shaped grains in the microstructure can only be attributed to cavitation-enhanced heterogeneous nucleation, since dendrite fragmentation would not be possible at those temperatures since the alloy was not on a mushy state. Grain refinement efficiency at different temperatures can be explained by the survival time of the acoustically induced nuclei. In fact, the developed nuclei are highly

thermodynamically instable (they form at the interfaces between the cavitation bubbles and the melt during the expansion stage of the bubbles (Eskin, 1998) and dissolve in the melt when bubbles collapse. As higher the melt temperature as shorter the survival time of the formed nuclei, thus decreasing the quantity of embryos in the melt and the number of globular grains in the final microstructure. As a consequence the number of active nuclei in the melt at 650ºC is higher than at 700ºC and the development of primary α-Al grains was easier, thus resulting in smaller grain sizes at 650ºC.

Independently of casting temperatures, the results of numerical simulation for the use of pressure curve (1) exhibited a filling velocity in the riser higher than 0.5m/s, which appears to be harmful by the presence of porosity in the microstructure, as can be observed in Fig. 7 (b and d). Indeed, the numerical simulations seems in agreement with experimental results as well as with the reported works which describe that there is a threshold velocity from which young oxides starts to be formed [20] and [21].

Fig. 7. Microstructure of samples at sensor #2 position (Fig. 2). (a) and (b) US degassed samples for casting temperature of 650ºC, for curves (2) and (1) respectively; (c) and (d) US degassed samples for casting temperature of 700ºC, for pressure curves (2) and (1) respectively; (e) and (f) non-US degassed samples for casting temperature of 650ºC and 700ºC, for curve (1) respectively

The fluid velocity behavior of filling is complex due to the pressure and geometry of castings. Thus, if the pressurizing rate (Pa/s) is increased, the resulting metal velocity tends to produce turbulence at the surface of the melt during filling of mould cavity (as suggested by figures 4b) and 5b)) due to the different liquid metal fronts and their subsequent contact with the mould walls. Besides, the existence of an open feeder to atmosphere showed to be problematic if pressure curve (1) is used because the melt can rise above the mould surface. The same figures clearly reveal that higher pressurizing rate (Pa/s) lead to an increase in the melt height which is favorable to filling the cavity in the form of "shower" that promotes breaking of the surface oxide film during metal drop. This evidence is in agreement with Runyoro *et al.* [21] who suggested that there is a maximum gate velocity above which the melt can rise as a jet sufficiently higher to fall back under gravity and during that stage the surface oxide film can be disrupted, folded and incorporated into the bulk of the melt.

To avoid the filling of cavity in form of "shower", during the first moments of casting, was proposed to use an intermediate ramp, which is characterized by pressure curve with 3 ramps (pressure curve (2)). The use of this pressure curve allowed decreasing the pressurized speed (Pa/s) in each moment promoting the filling of cavity smoothly with clean liquid from the bottom of the crucible, resulting in microstructures free from porosities and oxides (Fig. 7 (a,c)), which are beneficial to the performance of casting.

Furthermore, the comparison between Fig. 7 (a,b) and Fig. 7 (c,d) reveals a very large difference in the resultant microstructure after ultrasonic degassing . Ultrasonic degassing at lower temperature promotes a more globular microstructure avoiding grain growing with dendritic morphology. The results suggest that ultrasonic degassing of aluminium alloy at low temperature can be equivalent to perform an isothermal grain refinement processing over

time. In addition to degassing the Al melt, ultrasonic degassing tends to improve its homogeneity and density, besides activation the liquid metal, which can be extremely important and beneficial for casting concerning melt fluidity.

In what concerns to the mechanical properties characterization, tensile testing was carried out, as referred in section 3.2. Table 3 presents the tensile testing results, including ultimate tensile stress, yield strength and elongation, for every processing conditions.

	Curve 1			Curve 2		
Temperature (ºC)	UTS (Mpa)	YS (Mpa)	El (%)	UTS (Mpa)	YS (Mpa)	El (%)
650	212±14	185±7	1.8±0.4	253±9	215±5	2.4±0.2
700	200±14	180±7	1.5±0.4	228±10	200±6	2.0±0.3

It is clear that the mechanical behaviour of samples cast at 650ºC with pressure curve (2) are significantly higher than those properties obtained for the samples cast in the other processing conditions. The increase in tensile stress is due to the globular morphology of α-Al grains and the absence of porosities in the microstructure, which also lead to an increase in ductility. Moreover, ductility increase can also be a consequence of a small size of unmodified eutectic Si particles, which increase was inhibited by the increase in the number of boundaries of α-Al grains. This suggests that even without specific Si modification operation, the reduction in size of Si particles also played an important role in ductility increase. In fact, US treatment did not promote Si modification, since this effect occurs at temperatures around 580ºC, which is significantly lower than the US treatment temperatures that were used.

From the data of ultimate tensile strength, two-parameter Weibull distribution plot was constructed and is presented in Fig. 8. The threshold value for 650ºC (i.e. 244 MPa) obtained with pressure curve (2), is higher than that obtained with pressure curve (1) (i.e. 218 MPa). The same situation was verified for casting temperature of 700ºC, as also shown in Fig. 8. In fact,

the ultrasonic degassing treatment combined with control of cavity filling at low pressure clearly improved the Al7Si0.3Mg alloy mechanical properties.

Fig. 8. Two-parameters Weibull distribution for different casting temperatures and pressure-time curves.

According to Tiryakioglu *et al*. [22] there is a critical value for $R^2_{0.05}$ calculated by equation (8) that can be used to evaluate the goodness-of-fit, i.e the distribution of the mechanical testing data is indeed Weibull if R^2 of the linear regression from the Weibull probability analysis is higher than to $R^2_{0.05}$ ($R^2 > R^2_{0.05}$).

$$R^2_{0.05} = 1.0637 - \frac{0.4174}{n^{0.3}} \qquad (8)$$

In present study, the value of n (number of samples) is 20 and $R^2_{0.05}$=0.89. Thus, based on the R^2 values of curve fittings, the two-parameter plot is suitable for different filling velocities (different pressure-time curves).

Fig. 9 presents SEM observation of the fracture surfaces in the tensile test bars. Interdendritic shrinkage and oxides can be seen in fracture surfaces. In the case of fracture surface of the specimens obtained with pressure curve (1), for different casting temperatures, it is evident the presence of oxides. Although, SEM analysis of the fracture surfaces confirmed the presence of oxides, these appears in different situations, i.e. for lower casting temperatures, the distribution of oxides is wholly irregular and evenly distributed, as showed by Fig. 9(a). On the other hand, for high casting temperatures, the presence of young oxides can be observed on the interdendritic region, as shown in Fig. 9(b).

Fig. 9. SEM pictures from the fracture surface of tensile test bars cast at different temperatures with pressure curve (2). (a) 650ºC; (b) 700ºC.

According to the microstructures presented in Figs. 7 and 9 and the results of ultimate tensile strength, it is clear that both filling velocity and the ultrasonic degassing play major roles in controlling the as-cast microstructure, thus the mechanical properties and reliability of cast aluminium components. Results also demonstrate the important role played by the formation of oxide films during mould filling. In fact, results confirm the expectations indicated in the introduction, that the 'young' oxide films are closely related to melt surface turbulence. Thus, a reduction in surface turbulence will reduce the possibilities of free surface break-up and the entrapment of surface oxide films by the liquid metal.

5. Conclusions

The effect of combining smooth mould cavity filling and ultrasonic degassing by using the Low Pressure Sand Casting process with US melt treatment on the microstructure and mechanical properties of Al7Si0.3Mg alloy was investigated. The main conclusions can be drawn from the developed study:

- Besides melt degassing, the ultrasonic degassing treatment at lower temperatures favors the grain refinement of the α-Al primary phase when compared with treatment at higher temperatures, leading to globular microstructures with small grain size. In fact, at 650ºC ultrasonic degassing has a microstructure refinement potential similar to traditional chemical refinement routes.
- The pressurization rate, then the mould filling velocity, has great influence in the development of oxide films, which remain entrapped in the melt after solidification. Oxide formation can be avoided using pressurization curves than lead to melt velocities lower than 0.5 m/s.
- The significant improvement in microstructure, both in what concerns to the microstructure morphology and the absence of porosity and oxides promote an increase

in the ultimate tensile strength of the alloy, which reached 253 MPa for a pouring temperature of 650ºC.

- It was shown that increasing of filling velocity decreases the value of Weibull modulus.

Acknowledgments

This research was supported by FEDER/COMPETE funds and by national funds through FCT - Portuguese Foundation for Science and Technology and was developed on the aim of the research project PTDC/EME-TME/119658/2010 and the Post-Doctoral grant SFRH/BPD/76680/2011. Also, this work has been supported by the FCT in the scope of the project: UID/EEA/04436/2013.

References

[1] S.-G. Liu, F.-Y. Cao, X.-Y. Zhao, Y.-D. Jia, Z.-L. Ning, J.-F. Sun, Characteristics of mold filling and entrainment of oxide film in low pressure casting of A356 alloy, Mater. Sci. Eng. A. 626 (2015) 159–164. doi:10.1016/j.msea.2014.12.058.

[2] M.A. Irfan, D. Schwam, A. Karve, R. Ryder, Porosity reduction and mechanical properties improvement in die cast engine blocks, Mater. Sci. Eng. A. 535 (2012) 108–114. doi:10.1016/j.msea.2011.12.049.

[3] C. Reilly, N.R. Green, M.R. Jolly, The present state of modeling entrainment defects in the shape casting process, Appl. Math. Model. 37 (2013) 611–628. doi:10.1016/j.apm.2012.04.032.

[4] S. Sun, B. Yuan, M. Liu, Effects of moulding sands and wall thickness on microstructure and mechanical properties of Sr-modified A356 aluminum casting alloy, Trans. Nonferrous Met. Soc. China. 22 (2012) 1884–1890. doi:10.1016/S1003-6326(11)61402-7.

[5] D. Dispinar, S. Akhtar, A. Nordmark, M. Di Sabatino, L. Arnberg, Degassing, hydrogen and porosity phenomena in A356, Mater. Sci. Eng. A. 527 (2010) 3719–3725. doi:10.1016/j.msea.2010.01.088.

[6] D. Dispinar, J. Campbell, Porosity, hydrogen and bifilm content in Al alloy castings, Mater. Sci. Eng. A. 528 (2011) 3860–3865. doi:10.1016/j.msea.2011.01.084.

[7] C.H. Cáceres, B.I. Selling, Casting defects and the tensile properties of an Al- Si-Mg alloy, Mater. Sci. Eng. A. 220 (1996) 109–116. doi:doi:10.1016/S0921-5093(96)10433-0.

[8] H. Xu, X. Jian, T.T. Meek, Q. Han, Degassing of molten aluminum A356 alloy using ultrasonic vibration, Mater. Lett. 58 (2004) 3669–3673. doi:10.1016/j.matlet.2004.02.055.

[9] W. Khalifa, Y. Tsunekawa, M. Okumiya, Effect of ultrasonic melt treatment on microstructure of A356 aluminium cast alloys, Int. J. Cast Met. Res. 21 (2008) 129–134. doi:10.1179/136404608X361819.

[10] L. Zhang, D.G. Eskin, A. Miroux, L. Katgerman, Formation of microstructure in Al-Si alloys under ultrasonic melt treatment, Light Met. TMS. (2012) 999–1004.

[11] H. Puga, J. Barbosa, E. Seabra, S. Ribeiro, M. Prokic, The influence of processing parameters on the ultrasonic degassing of molten AlSi9Cu3 aluminium alloy, Mater. Lett. 63 (2009) 806–808. doi:10.1016/j.matlet.2009.01.009.

[12] K.C. Mills, Al - LM25, in: Recomm. Values Thermophys. Prop. Sel. Commer. Alloys, Woodhead Publishing, 2002: pp. 43–49.

[13] B. Zhang, D.M. Maijer, S.L. Cockcroft, Development of a 3-D thermal model of the low-pressure die-cast (LPDC) process of A356 aluminum alloy wheels, Mater. Sci. Eng. A. 464 (2007) 295–305. doi:10.1016/j.msea.2007.02.018.

[14] M. Zhu, Z. Jian, G. Yang, Y. Zhou, Effects of T6 heat treatment on the microstructure, tensile properties, and fracture behavior of the modified A356 alloys, Mater. Des. 36 (2012) 243–249. doi:10.1016/j.matdes.2011.11.018.

[15] M. Tiryakioğlu, J. Campbell, Weibull Analysis of Mechanical Data for Castings: A Guide to the Interpretation of Probability Plots, Metall. Mater. Trans. A. 41 (2010) 3121–3129. doi:10.1007/s11661-010-0364-6.

[16] J.B. Quinn, G.D. Quinn, A practical and systematic review of Weibull statistics for reporting strengths of dental materials, Dent. Mater. 26 (2010) 135–147. doi:10.1016/j.dental.2009.09.006.

[17] J.A. Hines, Determination of interfacial heat-transfer boundary conditions in an aluminum low-pressure permanent mold test casting, Metall. Mater. Trans. B. 35 (2004) 299–311.

[18] X. LI, Q. HAO, W. JIE, Y. ZHOU, Development of pressure control system in counter gravity casting for large thin-walled A357 aluminum alloy components, Trans. Nonferrous Met. Soc. China. 18 (2008) 847–851. doi:10.1016/S1003-6326(08)60147-8.

[19] H. Puga, J. Barbosa, J.C. Teixeira, M. Prokic, A New Approach to Ultrasonic Degassing to Improve the Mechanical Properties of Aluminum Alloys, J. Mater. Eng. Perform. 23 (2014) 3736–3744. doi:10.1007/s11665-014-1133-2.

[20] M. Jolly, Prof. John Campbell's ten rules for making reliable castings, JOM. 57 (2005) 19–28.

[21] J.J. Runyoro, S.M.A. Boutorabi, J. Campbell, Critical Gate Velocities for Film Forming Alloys: A Basis for Process Specification, Trans. AFS, 1992.

[22] M. Tiryakioğlu, D. Hudak, G. Ökten, On evaluating Weibull fits to mechanical testing data, Mater. Sci. Eng. A. 527 (2009) 397–399. doi:10.1016/j.msea.2009.08.014.

Figure Captions

Fig. 1. Model of casting layout.

Fig. 2. Geometric model where S#1 and S#2 are the sensors.

Fig. 3. Experimental set-up of LPSC process. (1) Electrical furnace; (2) Sealing cap; (3) US-degassing system; (4) Device for filling mould; (5) Pressurizing gas.

Fig. 4. Numerical results of mould filling simulation for 700 ºC casting temperature. (a) Average melt velocity of filling registered in sensor S#1 during cavity filling; (b) flow chart of velocity in cavity for a filling of 70%.

Fig. 5. Numerical results of mould filling simulation for 650 ºC casting temperatures. (a) Average melt velocity of filling registered in sensor S#1 during cavity filling; (b) flow chart of velocity in cavity for a filling of 70%.

Fig. 6. Average density of the Al7Si0.3Mg as a function of melt temperature and processing time, for 20.1±0.1 kHz and 40 μm of the amplitude of system, evaluated for all experiments.

Fig. 7. Microstructure of samples at sensor #2 position (Fig. 2). (a) and (b) casting temperature of 650ºC, for curves (2) and (1) respectively; (c) and (d) casting temperature of 700ºC, for pressure curves (2) and (1) respectively.

Fig. 8. Two-parameters Weibull distribution for different casting temperatures and pressure-time curves.

Fig. 9. SEM pictures from the fracture surface of tensile test bars cast at different temperatures with pressure curve (2). (a) 650ºC; (b) 700ºC.

Tables

Table 1. Parameters of the pressure-time (p-t) curves used for mould filling.

Pressure curve	M1 (0 – 5 s)	M2 (5 – 10 s)	M3 (10 – 15 s)	M4 (15– … s)	Observation
(1)	1400 Pa/s	400 Pa/s	0	0	Curve with 2 ramps
(2)	600 Pa/s	400 Pa/s	800 Pa/s	0	Curve with 3 ramps

Table 2. Experimental conditions.

Test Nº.	Temperature (ºC)	Ultrasonic parameters			Pressure curve (see Table 1)
		Time (min)	Frequency (kHz)	Amplitude (μm)	
1	650	0-1-3-5-9	20.1±0.1	40	(2)

2				(1)
3	700	0-1-3-5		(2)
4				(1)